Annealing of silicon heterojunction solar cells: Interplay of solar cell and Indium-Tin-Oxide properties

Jan Haschke, Raphaël Lemerle, Brahim Aïssa, Amir A. Abdallah, Maulid M. Kivambe, Mathieu Boccard, and Christophe Ballif

***Abstract*—We report on the evolution of silicon heterojunction solar cell properties focusing in particular on the Indium-Tin-Oxide (ITO) layers upon consecutive thermal annealing. We find that the charge carrier density N_e of the ITO increases with higher thermal budget while the carrier mobility stays constant. For the solar cells, their series resistance at maximum power point $R_\mathrm{S}^\mathrm{MPP}$ first decreases due to the reduction of the ITO's sheet resistance. With further annealing, $R_\mathrm{S}^\mathrm{MPP}$ increases again. As all monitored R_S components decrease, we attribute this to an increase of the contact resistance. The implied V_OC as well as the implied fill-factor both slightly degrade for annealing temperatures above 190 °C for our layers. This, as well as the change in N_e of the ITO, must be carefully considered when optimising the thermal budget needed e.g. for sputter damage or screen-printing paste curing.**

***Index Terms*—series resistance, loss analysis, refractive index, ITO, sputter damage, selectivity, silicon heterojunction.**

I. Introduction

In two-side contacted silicon heterojunction (SHJ) solar cells, a transparent conductive oxide (TCO) is usually applied at the front-side, as the sheet resistance of the amorphous silicon layers is too high for low-loss lateral current transport [1]. The TCO needs to be as transparent as possible in the UV-vis-NIR range [2], and highly conductive to provide low lateral resistivity. In SHJ solar cells, usually Indium-based TCOs and in particular Indium-Tin-Oxide (ITO) [3] are used as standard in industry. Besides tin and oxygen vacancies, hydrogen can also act as a donor for Indium-based TCOs [4], [5] and provide additional electrons, increasing the charge carrier density in the ITO. It has been reported that annealing of ITO deposited on amorphous silicon can drastically increase its carrier density [6]. Also, with the emergence of screen-printing pastes that are already sufficiently conductive after annealing at 130 °C, and the requirement for some of the non-Si selective contacts (like MoO_x, TiO_x, [7]) to not be cured at too high temperatures, it is relevant to know at which minimal temperature an SHJ cell has to be annealed in order to perform optimally.

In this paper, we investigate the interplay of SHJ solar cell properties with its ITO layers upon consecutive thermal annealing between 130 °C and 210 °C. We analyse the series-resistance components at each annealing step and link the optical and electrical parameters of the ITO to the solar cell's JV parameters.

II. Experimental

Five two-side contacted 2x2 cm^2 SHJ solar cells were prepared on a two-side textured 180 µm 2 Ω cm n-type FZ-wafer with (100) orientation. A schematic of the cell structure is sketched in Fig. 1a. All silicon layers were deposited by plasma enhanced chemical vapor deposition (PECVD) in a parallel-plate plasmabox KAI-M system at 200 °C. The ITO layers were deposited at room temperature via reactive DC sputtering, with a process pressure of 8 mTorr, and a power density of ≈2 W cm^{-2}, in an MRC-II system. The target composition was In_2O_3(90):SnO_2(10), and the O_2/Ar ratio during depostion 0.02 (ITO front), and 0.03 (ITO back), respectively. The different thicknesses of ITO front (≈115 nm[1]), and ITO back (≈230 nm[1]) were obtained by varying the speed of the substrate holder moving in front of the vertical target during deposition. Both systems feature large-area (>30 cm × 30 cm) deposition. At the rear side, a Ag layer is sputtered, and on the front side a Ag grid is screen-printed. Additionally, a specific sample for the measurement of the minority charge carrier lifetime was prepared, using the same processes as for the solar cells, but omitting the Ag front and rear metallisation, to allow for lifetime measurements. For Hall measurements of the ITO, dedicated planar samples on glass were prepared, using the same deposition conditions for silicon and ITO layers as for the solar cells. The thickness of the *a*-Si:H(i/p), and *a*-Si:H(i/n)/*nc*-Si:H(n) stacks on glass are 20 nm and 40 nm, respectively. For the analysis of ITO front and back, two samples have been prepared for each case. Measurements were not performed after each annealing, but only for selected steps. When data was available from two samples, the average value and standard deviation were calculated.

[1]on planar reference glass

Manuscript received March 22, 2019; revised May 13, 2019 and June 11,2019; accepted June 13, 2019.

J. Haschke, R. Lemerle, M. Boccard, and C. Ballif are with Ecole Polytechnique Fédérale de Lausanne, Institute of Microengineering (IMT), Photovoltaics and Thin-Film Electronics Laboratory (PV-lab), Rue de la Maladière 71B, CH-2002 Neuchâtel, Switzerland.

B. Aïssa, A. A. Abdallah, and M. M. Kivambe are with Qatar Environment and Energy Research Institute (QEERI), Hamad bin Khalifa University, Qatar Foundation, P.O. Box 5825, Doha, Qatar.

doi: https://dx.doi.org/10.1109/JPHOTOV.2019.2924389

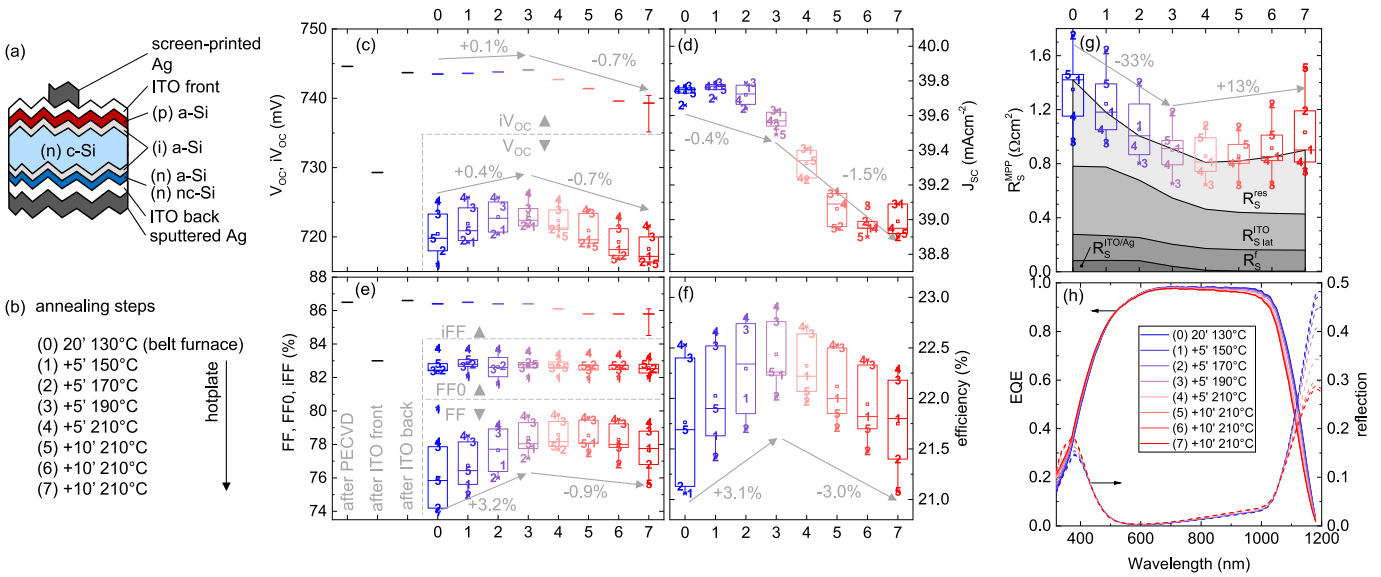

Fig. 1. (a) Schematic of the device structure, (b) list of consecutive annealing steps, (c)-(f) JV parameter of five SHJ solar cells undergoing annealing, (g) break-down of series resistance components, (h) external quantum efficiency and reflection. The slopes of the grey arrows are matching the slopes of the average values, the grey numbers indicate the relative change with respect to the value at steps (0) and (3) respectively.

The lifetime measurements were performed on a Sinton Instruments WCT-120TS [8] tool at the center of the wafer. To estimate the deviation, the lifetime was measured at five positions on the wafer after annealing step (7). The five positions correspond to the positions of the cells. The relative deviation of iV_{OC} and *iFF* towards the values at the center is shown as y-error for step (7) and assumed to be similar for all annealing steps. JV measurements of the solar cells were performed at 25 °C with a dual-lamp Wacom AM1.5g solar simulator with AAA characteristics. Two JV measurements were performed, at 100 mW cm^{-2}, and 5.5 mW cm^{-2} intensity, and the series-resistance-free fill-factor FF_0, as well as the series resistance at maximum power point R_S^{MPP} were calculated following the method of Bowden *et al.* [9]. From a transfer-length (TLM) structure [10] on the same wafer as the solar cells, the sheet resistance of the front ITO as well as the contact resistance between ITO and the screen-printed Ag grid were calculated. The line resistance of the grid fingers was obtained measuring the resistance between the two external busbars and dividing by the number of fingers. Spectroscopic ellipsometry measurements for ITO on Si-coated glass were performed on a HORIBA Jobin Yvon, UVISEL ellipsometer. From fitting with a Tauc-Lorentz/Drude model, the thickness, the refractive index n as well as the extinction coefficient k were obtained. Hall measurements were performed with a HMS-5000 system using the van der Pauw method.

The initial annealing of the samples (20 min at 130 °C) was carried out in a belt furnace. Subsequent consecutive annealings up to 210 °C were performed on a Präzitherm hotplate in air. The list of annealing steps is shown in Fig. 1b. After each annealing, the above mentioned measurements were performed on the respective samples.

III. Results & Discussion

A. Solar cell parameters

In Figs. 1c-f we show boxplots of the JV parameters after each of the consecutive annealing steps. The numbers in the boxplot indicate the cell. The implied values for open-circuit voltage and fill-factor, iV_{OC} and *iFF*, are also included in Figs. 1c and e respectively. For the implied values, we added also the steps "after PECVD", "after ITO front", and "after ITO back". Figs. 1c and e show that sputter-induced damage [11], [12], is introduced with the deposition of the ITO at the front, which can be seen in reduced iV_{OC} and *iFF* values "after ITO front". With the deposition of the rear side ITO, the sputter-induced damage is largely cured. Although no intentional heating is applied during sputtering, the sample heats up during the deposition, which could cause hydrogen to become mobile and (re-)passivate dangling bonds. The *a*-Si:H(i/n)/*nc*-Si:H(n) stack at the rear side seems to be thick enough to prevent any sputter-induced damage during the deposition of "ITO back". With further annealing, iV_{OC} first stays constant and then marginally increases up to step (3). The average of the open-circuit voltage V_{OC} also increases from step (0) to step (3), but the increase is slightly higher than for the iV_{OC}. This means that the increase in V_{OC} cannot be solely attributed to improved passivation. Possibly, the activation energy of the *a*-Si:H(p) layer is reduced upon annealing [13] due to a reduction of the defect-density [14], [15] from (0) to (3), which could lead to an increased selectivity and thus higher V_{OC}. With further annealing, V_{OC} decreases due to a loss in passivation as iV_{OC} decreases as well. We attribute this to out-diffusion of hydrogen from *a*-Si:H(i) and thus increased dangling-bond density [16].

The short-circuit current density J_{SC} decreases from step (2) to (6) by about 0.8 mA cm^{-2}. This decrease is mainly due to reduced spectral response >800 nm, as was calculated from

the external quantum efficiency (EQE), which are shown in Fig. 1h. This is mainly due to increased parasitic absorption, which is indicated by the decreased reflection at 1200 nm (cf. Fig. 1h) [17], and the extinction coefficient k of the ITO which increases with annealing for wavelengths >500 nm as can be seen in Fig. 2d. This increase is due to the increase of N_e (cf. next section), for both ITO front and back.

The fill-factor *FF* increases until step (4) and then slightly decreases. These changes are essentially driven by a change of the devices' $R_\mathrm{S}^\mathrm{MPP}$, as FF_0 decreases only marginally. The *iFF* decreases slightly stronger. This could be due to process variations (lifetime sample and cells were processed on different wafer batches, and in different deposition runs), due to inaccuracy of the FF_0 determination, or an impact of the metallisation (Ag grid & rear side) of the solar cells.

$R_\mathrm{S}^\mathrm{MPP}$ is shown in Fig. 1g, together with a breakdown of the R_S components:

- lateral transport in the ITO $R_\mathrm{S,lat}^\mathrm{ITO}$,
- transport in the front-grid fingers R_S^f, and
- the contact resistance between ITO and the screen-printed Ag $R_\mathrm{S}^\mathrm{ITO/Ag}$.

$R_\mathrm{S,lat}^\mathrm{ITO}$ and R_S^f are obtained as described in the appendix in equations (1) and (2). $R_\mathrm{S,lat}^\mathrm{ITO}$ decreases until step (4) and stays constant for further annealing. The finger resistance R_S^f is not affected by the annealing. $R_\mathrm{S}^\mathrm{ITO/Ag}$ was obtained from the TLM measurements/equation (3), and becomes negligible after step (3). The share of all components is shown in grey scales in Fig. 1g. The decrease of $R_\mathrm{S,lat}^\mathrm{ITO}$ i.e. $R_\mathrm{sheet}^\mathrm{ITO}$ is driven by the increase of the free carrier concentration N_e in the ITO (cf. next section), and responsible for the reduction of $R_\mathrm{S}^\mathrm{MPP}$ from step (0) to (3). Subtracting $R_\mathrm{S,lat}^\mathrm{ITO}$, R_S^f, and $R_\mathrm{S}^\mathrm{ITO/Ag}$ from the median of $R_\mathrm{S}^\mathrm{MPP}$, gives the residual R_S ($R_\mathrm{S}^\mathrm{res}$). It increases after its minimum at step (2), and amounts to roughly half of the $R_\mathrm{S}^\mathrm{MPP}$ at step (7). $R_\mathrm{S}^\mathrm{res}$ includes the unknown R_S components contact resistance at the front (*c*-Si(n)/*a*-Si:H(i/p)/ITO), and at the back (*c*-Si(n)/*a*-Si:H(i/n)/*nc*-Si:H(n)/ITO). Its increase from step (3) to step (7) is thus likely indicating a change in contact resistance. It has to be noted though that the increase of $R_\mathrm{S}^\mathrm{res}$ might not be as pronounced as derived from our analysis. Besides the ITO, also the wafer is providing lateral conductance at MPP [18], which we did not take into account here[2]. As this becomes more important with higher sheet resistance of the ITO, it would lower the R_S for lateral conduction especially for the steps (0)-(3) where the sheet resistance of the ITO is comparably high (cf. Fig 2c), leading to a lower increase of $R_\mathrm{S}^\mathrm{res}$.

Nevertheless, $R_\mathrm{S}^\mathrm{MPP}$ increases from (4) to (7), indicating that an increase in contact resistance is still happening. As contact properties are a result of an interplay of all layers (*a*-Si:H(i), doped *a*-Si:H, ITO), the exact determination of what is causing the increase is challenging. A change in workfunction of the ITO could play a role [20]–[23], a reduction of the conductivity of the doped layer, possibly due to annealing [24], or a combination, as both are linked [23], [25]. We expect the deterioration to happen at the p-contact and not at the n-contact, as generally *nc*-Si:H(n) features lower E_a compared with *a*-Si:H(p).

The observed phenomena occur with our *a*-Si:H-layers. Different processes for the deposition of *a*-Si:H might be more or less affected by thermal annealing [26].

To summarise, from step (0) to step (3), the increase of the efficiency η is mainly driven by the increase in *FF*, the increase in V_OC is compensated by the decrease in J_SC. From step (3) to step (7) all parameters decrease, with the J_SC being the main driver.

B. ITO parameters

In Fig. 2 we show how the ITO properties change with annealing. The charge carrier concentration $N_\mathrm{e}^\mathrm{Hall}$ and the mobility $\mu_\mathrm{e}^\mathrm{Hall}$ were obtained from Hall measurements of the planar layers on glass/Si and are shown in Figs. 2a and b respectively. N_e increases with annealing for both ITO front and ITO back. The increase is more pronounced for ITO back which also starts from a lower value due to the higher O_2/Ar ratio during the deposition. The mobility stays constant for both ITO front and back (cf. Fig. 2b). From Fig. 2c it can be seen that $R_\mathrm{sheet}^\mathrm{ITO}$ of the front ITO is mainly driven by N_e as it decreases with annealing, especially until step (4) and then saturates, similarly to N_e. In the figure, we show two values for $R_\mathrm{sheet}^\mathrm{ITO}$, one directly measured on the wafer via TLM, and the other calculated from $N_\mathrm{e}^\mathrm{Hall}$ and $\mu_\mathrm{e}^\mathrm{Hall}$ using equation (4) in the appendix. Within the experimental uncertainties, both values are in good agreement, indicating that the samples on glass represent well the situation on wafer. Fig. 2d shows the refractive index n and the extinction coefficient k of the ITO front. The refractive index n decreases with subsequent annealing. The extinction coefficient k, shown in Fig. 2d, indicates a Burstein-Moss-shift and increased free carrier absorption, both as a result of the increasing N_e with annealing.

As shown in literature [27], for ITOs deposited with different O_2/Ar ratios, n decreases with increasing N_e. Our results confirm that this change is also observed for other mechanisms that increase N_e (in our case most probably doping with hydrogen from the underlying *a*-Si:H layers or oxygen effusion [3], [6], [28]). The increase in n is the reason for the slightly increased reflection of the solar cells in the visible range, as shown in Fig. 1h, and verified with OPAL2 simulations (not shown).

IV. Conclusions

We presented the interplay between ITO and silicon heterojunction (SHJ) solar cell properties upon thermal annealing. The main driver behind the observed changes is the increase of the free carrier concentration in the ITO that impacts mainly the short-circuit current density of the device, but also the fill-factor as a result of the change in sheet-resistance of the front-side ITO $R_\mathrm{sheet}^\mathrm{ITO}$. Depending on the thermal budget required by the SHJ solar cell device for e.g. curing of sputter damage or the screen-printing paste, the ITO properties have to be carefully tuned accordingly. We found that with

[2]The resistance due to vertical transport is also injection-dependent [19] and could thus further complicate the analysis. However, we estimate it to be below $0.1\,\Omega\,\mathrm{cm}^2$ and thus did not consider it.

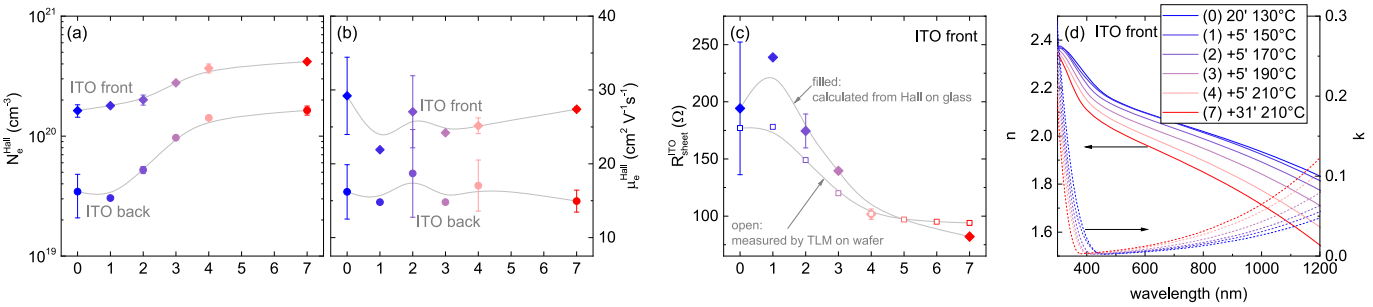

Fig. 2. (a) Charge carrier density and (b) mobility of planar ITO layers deposited on silicon on glass. (c) Sheet resistance of ITO front as measured by TLM on the same wafer as the solar cells, and calculated from the Hall measurements of the planar samples (cf. equation (4) in the appendix). (d) Refractive index n, and extinction coefficient k of ITO front. ITO front refers to an O_2/Ar ratio of 0.02, deposited on a stack of a-Si:H(i)/a-Si:H(p), and a thickness of 112-114 nm on the planar glass sample. ITO back refers to an O_2/Ar ratio of 0.03, deposited on a stack of a-Si:H(i)/a-Si:H(n)/nc-Si:H(n), and a thickness of 237 nm on the planar glass sample. The numbers refer to the same annealing steps as listed in Fig. 1b. The grey lines are B-splines as guide to the eye.

annealing, the series resistance at the maximum power point first decreases due to a reduction in $R_{\mathrm{sheet}}^{\mathrm{ITO}}$, but increases again with prolonged annealing. This has not been fully understood yet and requires further examination. As annealing above 190 °C lead to a slight decrease in passivation (seen from a reduction of implied V_{OC} and fill-factor), it should ideally be avoided for our SHJ solar cells.

Appendix

Calculation of R_{S} components

In Fig. 3 we illustrate the unit cell of our SHJ solar cell. We also show the parameters used to calculate the series resistant components shown in Fig. 1g with the equations (1)-(3), which we define below.

From the sheet resistance of the ITO $R_{\mathrm{sheet}}^{\mathrm{ITO}}$, obtained from TLM as described above, and the distance between two fingers p, the R_{S} component (normalised to the area, $[R_{\mathrm{S}}]{=}\Omega\,\mathrm{cm}^2$) due to lateral current conduction in the ITO can be calculated with

$$R_{\mathrm{S,lat}}^{\mathrm{ITO}} = \frac{1}{12}\, p^2\, R_{\mathrm{sheet}}^{\mathrm{ITO}} \ . \tag{1}$$

From the resistance between the two external busbars and equation 2, the finger resistance can be calculated with the line resistance of a finger $R_{\mathrm{line}}^{\mathrm{f}}$ in $\Omega\,\mathrm{cm}^{-1}$, and the finger length l_{f}

$$R_{\mathrm{S}}^{\mathrm{f}} = \frac{1}{3}\, p\, l_{\mathrm{f}}^2\, R_{\mathrm{line}}^{\mathrm{f}} \ . \tag{2}$$

From the specific contact resistance between the screen-printed Ag and the ITO $\rho_{\mathrm{C}}^{\mathrm{ITO/Ag}}$, as well as the ratio of front-grid area (A_{grid}) and cell area (A_{cell}), the contact resistance between front-grid and ITO front can be calulated with

$$R_{\mathrm{S}}^{\mathrm{ITO/Ag}} = \rho_{\mathrm{C}}^{\mathrm{ITO/Ag}} \cdot \frac{A_{\mathrm{grid}}}{A_{\mathrm{cell}}}, \ \text{with} \ \frac{A_{\mathrm{grid}}}{A_{\mathrm{cell}}} = 0.025. \tag{3}$$

The $R_{\mathrm{sheet}}^{\mathrm{ITO}^*}$ was calculated from the Hall measurements (layers on planar glass samples) using the charge carrier density $N_{\mathrm{e}}^{\mathrm{Hall}}$, the mobility $\mu_{\mathrm{e}}^{\mathrm{Hall}}$, the thickness t_{ITO}, and the elementary charge q with the following equation

$$R_{\mathrm{sheet}}^{\mathrm{ITO}^*} = \frac{1}{q N_{\mathrm{e}}^{\mathrm{Hall}} \mu_{\mathrm{e}}^{\mathrm{Hall}}} \frac{1}{t_{\mathrm{ITO}}} \cdot 1.7 \ . \tag{4}$$

The geometry factor of 1.7 accounts for the lower thickness of the ITO on wafer compared with the layers on planar glass, to establish comparability with the $R_{\mathrm{sheet}}^{\mathrm{ITO}}$ obtained from the TLM on wafer.

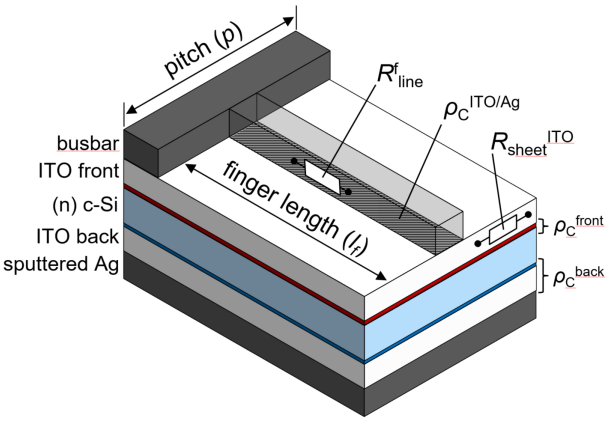

Fig. 3. Unit cell sketch of the SHJ solar cell investigated in this study. The parameters used to calculate the different series resistance components are indicated. $R_{\mathrm{S}}^{\mathrm{res}}$ (cf. Fig. 1g) includes ρ_C^{front}, ρ_C^{back}, and other resistances.

Acknowledgment

The authors acknowledge Christophe Allebé, Patrick Wyss, and Nicolas Badel from CSEM for high quality wet-processing and metallization. The Qatar Foundation is acknowledged for funding. Funding from the Swiss National Science Foundation (SNF) through the Ambizione Energy grant "ICONS" is also acknowledged.

References

[1] J. Haschke, O. Dupré, M. Boccard, and C. Ballif, "Silicon heterojunction solar cells: Recent technological development and practical aspects - from lab to industry," *Solar Energy Materials and Solar Cells*, vol. 187, no. July, pp. 140–153, dec 2018.

[2] M. Morales-Masis, S. De Wolf, R. Woods-Robinson, J. W. Ager, and C. Ballif, "Transparent Electrodes for Efficient Optoelectronics," *Advanced Electronic Materials*, vol. 3, no. 5, 2017.

[3] R. Bel Hadj Tahar, T. Ban, Y. Ohya, and Y. Takahashi, "Tin doped indium oxide thin films: Electrical properties," *Journal of Applied Physics*, vol. 83, no. 5, pp. 2631–2645, 1998.

[4] T. Koida, H. Fujiwara, and M. Kondo, "Hydrogen-doped In2O3 as High-mobility Transparent Conductive Oxide," *Japanese Journal of Applied Physics*, vol. 46, no. No. 28, pp. L685–L687, jul 2007. [Online]. Available: http://stacks.iop.org/1347-4065/46/L685

[5] S. Limpijumnong, P. Reunchan, A. Janotti, and C. G. Van De Walle, "Hydrogen doping in indium oxide: An ab initio study," *Physical Review B - Condensed Matter and Materials Physics*, vol. 80, no. 19, pp. 1–4, 2009.
[6] K.-U. Ritzau, T. Behrendt, D. Palaferri, M. Bivour, and M. Hermle, "Hydrogen doping of Indium Tin Oxide due to thermal treatment of hetero-junction solar cells," *Thin Solid Films*, vol. 599, pp. 161–165, jan 2016. [Online]. Available: http://www.sciencedirect.com/science/article/pii/S0040609015012778https://linkinghub.elsevier.com/retrieve/pii/S0040609015012778
[7] J. Bullock, Y. Wan, M. Hettick, J. Geissbuhler, A. J. Ong, D. Kiriya, D. Yan, T. Allen, J. Peng, X. Zhang, C. M. Sutter-Fella, S. De Wolf, C. Ballif, A. Cuevas, and A. Javey, "Survey of dopant-free carrier-selective contacts for silicon solar cells," in *Conference Record of the IEEE Photovoltaic Specialists Conference*, vol. 2016-Novem, 2016, pp. 210–214.
[8] J. Schmidt and R. A. Sinton, "Defect Characterization by Temperature and Injection-dependent Lifetime Spectroscopy," *Proceedings of the 3rd World Conference on Photovoltaic Energy Conversion*, p. 3001, 2003.
[9] S. Bowden and A. Rohatgi, "Rapid and accurate determination of series resistance and fill factor losses in industrial silicon solar cells," *17th European Photovoltaic Solar Energy Conference*, 2001. [Online]. Available: https://smartech.gatech.edu/handle/1853/26165http://smartech.gatech.edu/handle/1853/26165
[10] H. H. Berger, "Models for contacts to planar devices," *Solid State Electronics*, vol. 15, no. 2, pp. 145–158, 1972.
[11] D. Zhang, A. Tavakoliyaraki, Y. Wu, R. A. Van Swaaij, and M. Zeman, "Influence of ITO deposition and post annealing on HIT solar cell structures," *Energy Procedia*, vol. 8, no. April, pp. 207–213, 2011.
[12] B. Demaurex, S. D. Wolf, A. Descoeudres, Z. C. Holman, and C. Ballif, "Damage at hydrogenated amorphous/crystalline silicon interfaces by indium tin oxide overlayer sputtering," *Applied Physics Letters*, vol. 101, no. 17, p. 171604, oct 2012. [Online]. Available: http://scitation.aip.org/content/aip/journal/apl/101/17/10.1063/1.4764529
[13] J. Jang, T. M. Kim, J. K. Hyun, J. H. Yoon, and C. Lee, "Temperature dependent light induced changes and annealing of the changes in hydrogen amorphous silicon," *Journal of Non-Crystalline Solids*, vol. 59-60, pp. 429–432, dec 1983.
[14] K. Shepard, Z. E. Smith, S. Aljishi, and S. Wagner, "Kinetics of the generation and annealing of deep defects and recombination centers in amorphous silicon," *Applied Physics Letters*, vol. 53, no. 17, pp. 1644–1646, oct 1988.
[15] N. Hata and S. Wagner, "A comprehensive defect model for amorphous silicon," *Journal of Applied Physics*, vol. 72, no. 7, pp. 2857–2872, oct 1992. [Online]. Available: https://doi.org/10.1063/1.351539http://aip.scitation.org/doi/10.1063/1.351539
[16] S. De Wolf, C. Ballif, and M. Kondo, "Kinetics of a-Si:H bulk defect and a-Si:H/c-Si interface-state reduction," *Physical Review B - Condensed Matter and Materials Physics*, vol. 85, no. 11, pp. 2–5, 2012.
[17] Z. C. Holman, M. Filipič, A. Descoeudres, S. D. Wolf, F. Smole, M. Topič, and C. Ballif, "Infrared light management in high-efficiency silicon heterojunction and rear-passivated solar cells," *Journal of Applied Physics*, vol. 113, no. 1, p. 013107, jan 2013. [Online]. Available: http://scitation.aip.org/content/aip/journal/jap/113/1/10.1063/1.4772975
[18] A. G. Aberle, G. Heiser, and M. A. Green, "Two-dimensional minority carrier flow in high-efficiency silicon solar cells at short-circuit, open-circuit and maximum power point operating conditions," *Solar Energy Materials and Solar Cells*, vol. 34, no. 1-4, pp. 149–160, sep 1994. [Online]. Available: http://linkinghub.elsevier.com/retrieve/pii/0927024894900353
[19] A. Cruz, E. C. Wang, A. B. Morales-Vilches, D. Meza, S. Neubert, B. Szyszka, R. Schlatmann, and B. Stannowski, "Effect of front TCO on the performance of rear-junction silicon heterojunction solar cells: Insights from simulations and experiments," *Solar Energy Materials and Solar Cells*, vol. 195, no. January, pp. 339–345, 2019. [Online]. Available: https://doi.org/10.1016/j.solmat.2019.01.047
[20] A. Kanevce and W. K. Metzger, "The role of amorphous silicon and tunneling in heterojunction with intrinsic thin layer (HIT) solar cells," *Journal of Applied Physics*, vol. 105, no. 9, p. 094507, 2009.
[21] S. Kirner, M. Hartig, L. Mazzarella, L. Korte, T. Frijnts, H. Scherg-Kurmes, S. Ring, B. Stannowski, B. Rech, and R. Schlatmann, "The Influence of ITO Dopant Density on J-V Characteristics of Silicon Heterojunction Solar Cells: Experiments and Simulations," *Energy Procedia*, vol. 77, pp. 725–732, aug 2015. [Online]. Available: http://www.sciencedirect.com/science/article/pii/S1876610215008711
[22] C. Messmer, M. Bivour, J. Schon, S. W. Glunz, and M. Hermle, "Numerical Simulation of Silicon Heterojunction Solar Cells Featuring Metal Oxides as Carrier-Selective Contacts," *IEEE Journal of Photovoltaics*, vol. 8, no. 2, pp. 456–464, mar 2018. [Online]. Available: http://ieeexplore.ieee.org/document/8291499/
[23] P. Procel, G. Yang, O. Isabella, and M. Zeman, "Theoretical evaluation of contact stack for high efficiency IBC-SHJ solar cells," *Solar Energy Materials and Solar Cells*, vol. 186, no. May, pp. 66–77, nov 2018. [Online]. Available: https://doi.org/10.1016/j.solmat.2018.06.021https://linkinghub.elsevier.com/retrieve/pii/S092702481830309X
[24] S. De Wolf and M. Kondo, "Boron-doped a-Si:Hc-Si interface passivation: Degradation mechanism," *Applied Physics Letters*, vol. 91, no. 11, pp. 1–4, 2007.
[25] M. Bivour, S. Schröer, and M. Hermle, "Numerical analysis of electrical TCO / a-Si:H(p) contact properties for silicon heterojunction solar cells," *Energy Procedia*, vol. 38, pp. 658–669, 2013. [Online]. Available: http://dx.doi.org/10.1016/j.egypro.2013.07.330http://www.sciencedirect.com/science/article/pii/S1876610213014161
[26] M. Boccard and Z. C. Holman, "Amorphous silicon carbide passivating layers for crystalline-silicon-based heterojunction solar cells," *Journal of Applied Physics*, vol. 118, no. 6, p. 065704, aug 2015. [Online]. Available: http://aip.scitation.org/doi/10.1063/1.4928203
[27] Z. Holman, A. Descoeudres, L. Barraud, F. Fernandez, J. Seif, S. De Wolf, and C. Ballif, "Current Losses at the Front of Silicon Heterojunction Solar Cells," *IEEE Journal of Photovoltaics*, vol. 2, no. 1, pp. 7–15, jan 2012.
[28] G. Frank and H. Köstlin, "Electrical properties and defect model of tin-doped indium oxide layers," *Applied Physics A Solids and Surfaces*, vol. 27, no. 4, pp. 197–206, 1982.

Jan Haschke received the Ph.D. degree in electrical engineering from the Technical University Berlin, Germany, in 2014. He is currently working as a postdoctoral research engineer with the Ecole Polytechnique Fédérale de Lausanne (EPFL) at PV-Lab, Neuchâtel, Switzerland. His research interests include development and understanding of high efficiency silicon heterojunction solar cell devices and fabrication processes.

Raphaël Lemerle received the bachelor degree in chemical engineering and is currently following the master program of material science and engineering at the Ecole Polytechnique Fédérale de Lausanne, Switzerland. He was working during a semester project with PV-Lab, Neuchâtel, Switzerland. He is specializing in energy conversion devices with a special focus on semiconductor materials.

Brahim Aïssa (Ph.D. Materials Science, INRS-EMT, University of Quebec, Canada, 2010) has extensive experience in the area of nanomaterials. He is fellow of the UNESCO Chair in Materials and Technologies for Energy Conversion, Saving and Storage. His activities focus on the growth, synthesis, processing and characterization of advanced materials and their integration into electronic and photonic devices. He has worked for MPB Communications, Inc., Space & Photonics Division from 2009 to 2014. He has authored more than 100 refereed journal papers, 3 books, 8 book-chapters, and holds two patents. He is currently a Senior Scientist in the Energy Conversion Group at Qatar Environment and Energy Research Institute (QEERI), at Hamad Bin Khalifa University (HBKU), Qatar Foundation (QF), and associate professor at College of Science and Engineering, HBKU, QF.

Amir A. Abdallah is a Scientist in the Energy Conversion Group at Qatar Environment and Energy Research Institute (QEERI), at Hamad Bin Khalifa University (HBKU), Qatar Foundation, in Doha, Qatar. After completing his MSc in mechanical engineering from Delft University of Technology (The Netherlands) he obtained his PhD in Material Science from Eindhoven University of Technology, Eindhoven (The Netherlands) in 2007. Dr. Abdallah has industrial experience in fabrication of silicon solar cells. This includes process optimization and characterization. In addition, he has experience in tackling the electronic properties of amorphous silicon thin film solar cells. Dr. Abdallah is coordinating the project activities in photovoltaic module performance and reliability. This includes power losses due to soiling and high operating temperature and module degradation.

Maulid M. Kivambe is a Scientist in the Energy Conversion Group at Qatar Environment and Energy Research Institute (QEERI), at Hamad Bin Khalifa University (HBKU), Qatar Foundation, in Doha, Qatar. He received his M.Sc. in Condensed Matter Physics and Biophysics in 2008, and his PhD in Materials Science and Engineering in 2012, both from the Norwegian University of Science and Technology (NTNU). He then worked as a postdoctoral associate at the Photovoltaics Research laboratory, Massachusetts Institute of Technology (MIT) for two years. His research interest is on structural, optical and electronic properties of materials for photovoltaic applications.

Mathieu Boccard received his Ph.D. from EPFL, PV-Lab in 2012 for his work on thin-film-silicon tandem solar cells. He then joined ASU, Tempe (USA) for a postdoc working on high-efficiency crystalline silicon, CdTe-based and perovskite/silicon tandem solar cells. Since 2017, he is leading the silicon heterojunction activities in EPFL, PV-Lab, working on fundamentals and novel materials for carrier-selective contacts, multijunction devices and location-dependent solar cell design.

Christophe Ballif received his Ph.D. from EPFL, Switzerland, in 1998. In 2004 he became a full professor with the Institute of Microengineering at the University of Neuchâtel, where he directs the Photovoltaics and Thin-Film Electronics Laboratory (PV-Lab), which is now part of EPFL. Since 2013 he has also been the director of the CSEM PV-center. His research interests include materials for PV, high-efficiency c-Si solar cells, module technology, BIPV and energy systems.